Korean J. Chem. Eng., **25**(6), 1286-1291 (2008)

Hydrothermal synthesis and characterization of Fe(III)-substituted mordenites

Yong Sig Ko*,†, Hyun Tae Jang, and Wha Seung Ahn*****

*Department of Advanced Material Chemistry, Shinsung University, Dangjin-gun 343-861, Korea
**Department of Chemical Engineering, Hanseo University, Seosan 356-706, Korea
***Department of Chemical Engineering, College of Engineering, Inha University, Incheon 402-751, Korea
(*Received 13 February 2008 • accepted 29 March 2008*)

Abstract−Fe-substituted mordenites were synthesized hydrothermally, partially substituting iron atoms for the framework aluminum of mordenite. XRD, SEM, IR, UV-VIS DRS, ESR, XAS, and catalytic activity studies provided the evidence of Fe^{3+} present in the zeolite framework. The framework IR bands were shifted to lower frequencies as Fe^{3+} ions incorporated into the lattice, and a new Si-O-Fe bond vibration was located near 668 cm^{-1}. The presence of a signal at g=4.3 in the ESR spectra was assigned to Fe^{3+} isomorphously substituted in the tetrahedral position. EXAFS at the Fe K-edge revealed that the Fe^{3+} ions were present in the zeolite framework in a four-fold coordination with an average Fe-O distance of 1.86 Å. In the UV-vis spectra, an absorption was observed at 375.7 nm which was assigned to the presence of Fe^{3+} in the zeolite framework. A toluene alkylation study reflected that the acidity strength of mordenite is weakened due to the presence of lattice iron species.

Key words: Mordenite, Iron, Isomorphous Substitution, Characterization, XAS

INTRODUCTION

The framework substitution of Si^{4+} and/or Al^{3+} by various transition metal ions into the framework of different zeolites has stimulated considerable interest in the utilization of zeolites as catalysts. Isomorphous substitution of Fe^{3+} into the framework of zeolites induces changes in acidity and modification in morphology, as well as pore expansion caused by introducing an Fe-O bond (1.84 Å) in the place of a Si-O bond (1.60 Å), which can affect the product selectivity. Dong et al. [1] incorporated Fe^{3+} into the mordenite framework and found that the iron-substituted mordenite had higher selectivity of isobutene than Al-mordenite for the dehydration of *tert*-butanol. Trace amounts of non-framework iron formed in the zeolites have also been shown to contribute to the overall catalytic activity [2].

Due to their interesting properties, zeolites isomorphously substituted with iron have been studied extensively [3-21]. Szostak and Thomas [3] were the first who deliberately synthesized a sodalite with significant quantities of Fe^{3+} in the framework (SiO_2/Fe_2O_3= 6-30). Over the years, a wide range of iron analogues such as SOD [4], MFI [5,6], MOR [8,9], MTT [10], MTW [11], LTL [12], IFR [13], BEA [14], VFI [15], ATS [16] and mesoporous silica molecular sieves [16-20] have been reported, and various characterization techniques employed to demonstrate the structural incorporated iron in these molecular sieves.

Synthetic mordenites are used extensively as catalysts and adsorbents. The replacement of Al^{3+} by Fe^{3+} ions in the mordenite framework may give rise to novel materials with interesting applications. Iron can be substituted into the tetrahedral framework sites of a molecular sieve structure during synthesis [3,22-24]; however, the amount of Fe^{3+} incorporated and the purity of the resulting zeolites depend on the conditions of synthesis [22]. Extra-framework iron species may be present in the as-synthesized materials; therefore care must be taken to avoid the formation of insoluble brown-colored ferric hydroxides [25].

Though synthesis methods of iron-substituted mordenites have been reported [7-9], further investigation concerning the synthesis of iron-substituted mordenites with extensive characterization and catalytic evaluation would contribute towards a better understanding of the system. In this work, we present the details of the synthesis procedure and characterization studies involving XRD, SEM, IR, EPR, UV-VIS DRS, and XAS for the zeolites having the MOR structure with associated iron species. Catalytic runs for toluene alkylation are also applied as a probe reaction to evaluate the property change.

EXPERIMENTAL

1. Synthesis

The reagents used in preparing the substrate were fumed silica (Cab-O-Sil, 97% SiO_2), sodium hydroxide (Junsei Co., 95%), sodium aluminate (Junsei Co., 32.6% Na_2O, 35.7% Al_2O_3), ferric nitrate nanohydrate (Shinyo Co., 98%), and deionized water. The Al- and Fe-substituted mordenite samples were synthesized from substrates having the following compositions: 7 Na_2O-x Fe_2O_3-(1−x) Al_2O_3-25 SiO_2-700 H_2O, where x=0, 0.15 and 0.30.

In a typical synthesis experiment, the reaction mixture was prepared by dissolving a desirable amount of ferric nitrate in deionized water to have solution A. Solution B was prepared by dissolving sodium hydroxide and sodium aluminate in deionized water. The required amount of fumed silica was added slowly to solution B with stirring until it was homogeneous. To this gel mixture solution A was slowly added with vigorous stirring until the homogeneous gel was obtained. The pH of the gel mixture was adjusted by the addition of dilute sulfuric acid aqueous solution to the desirable

†To whom correspondence should be addressed.
E-mail: ysko@shinsung.ac.kr

value (pH ≒ 10.5). The resulting pale yellow gel formed was further stirred for 1 h intensively. The reaction mixture was transferred to a 100 ml teflon-lined stainless steel autoclave and maintained in an air oven at 443 K under unstirred conditions. Autoclaves were removed at different time intervals from the oven and were quenched immediately in cold water for phase identification. After the solid products were suction-filtrated, excess alkali was washed out with deionized water and the products were dried in an air oven at 393 K for 12 h.

2. Characterization

X-Ray diffraction patterns of the different crystalline samples were determined by Philips, PW-1700 diffractometer using Ni-filtered monochromatic CuKα radiation, 40 kV, 25 mA with a scanning rate of 6° min^{-1} (2θ). The crystallite size and morphology of the crystalline phase were examined with a scanning electron microscope (Hitachi, X-650) after coating with a Au-Pd evaporated film. Framework IR spectra of the samples were recorded in air at room temperature on a Perkin Elmer 221 spectrometer (in the range of 400-4,000 cm^{-1}) with wafers of zeolites mixed with dry KBr. Electron spin resonance spectra were measured with a Bruker E-2000 spectrometer in the temperature range of 100 K-300 K. Diffuse reflectance UV-vis spectra were recorded with a Varian CARY 3E spectrometer equipped with an integrating sphere and dehydrated MgO as a reference in the range of 190-900 nm. The XAS spectra were measured above the Fe K-edge at beamline 10B, Photon Factory of National Laboratory for High Energy Physics in Tsukuba, Japan. EXAFS data were analyzed by using the UWXAFS2 program package [26]. The EXAFS oscillation (χ(k)) was multiplied by the wave vector cube (k^3) after background removal and normalization. The background was removed with R-space technique [27,28], which minimized low R components in its Fourier transform compared with the standard generated from FEFF5 code [29]. This procedure is described in detail elsewhere [27-30].

3. Catalytic Reaction Study

The H-forms of zeolites were obtained by ion-exchanging the zeolites prepared three times by the conventional procedure with 1 M ammonium nitrate aqueous solution at 368 K for 19 h, washed until no NO_3^- was detected, dried at 373 K overnight and calcined at 773 K for 3 h. Toluene alkylation with ethanol on the zeolites in their H^+-forms was carried out at atmospheric pressure at 623 K by using a conventional fixed bed microreactor with 0.1 g catalyst pretreated in a hydrogen stream for 2 h at 773 K. The liquid mixture (2 : 1 mole ratio) of toluene/ethanol was fed to the evaporator by a syringe pump, and the hydrogen carrier then transported the reactant to the microreactor. The reaction products were analyzed by on-line GC using a 4.5 m column packed with 5% Bentone-34 and 5% diisodecyl phthalate on Uniport B.

RESULTS AND DISCUSSION

The X-ray diffraction patterns of the crystals are shown in Fig. 1. Closely matching diffractograms of mordenite were obtained irrespective of the iron content of the sample. While the crystallization time was kept at 24 h for the iron free mordenite, that for the Fe-substituted mordenite samples was kept at 34 to 40 h in order to obtain the same level of crystallinity, as the iron content increased. No detectable iron oxide peaks were observed.

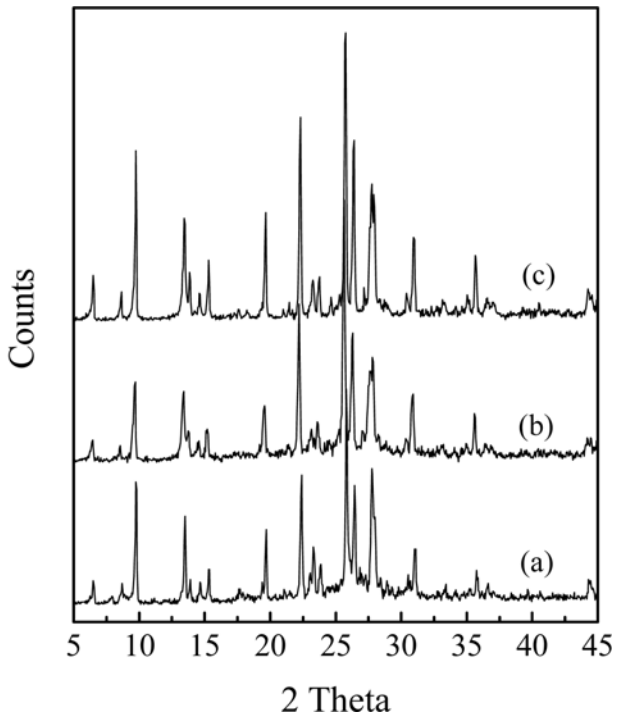

Fig. 1. X-ray diffraction patterns of Al- and Fe-substituted mordenite samples. (a) x=0.00, (b) x=0.15, and (c) x=0.30.

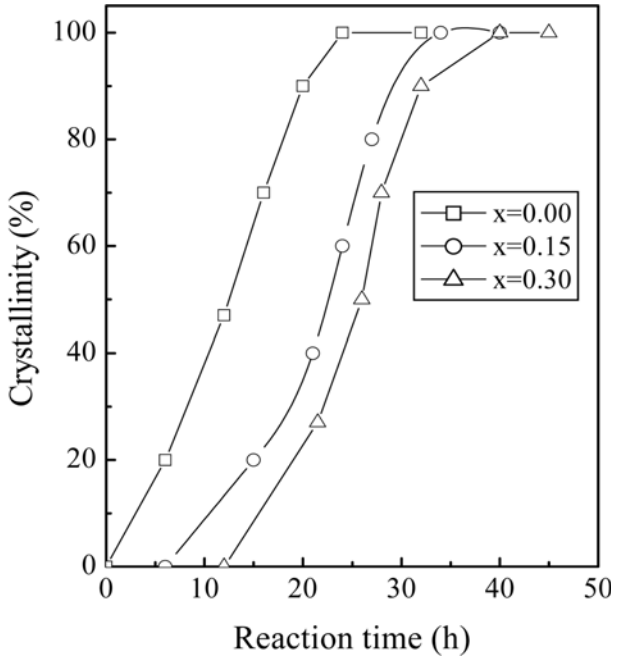

Fig. 2. Crystallization curves for Al- and Fe-substitution mordenite samples. Substrate composition: 7 Na_2O-x Fe_2O_3-(1−x) Al_2O_3-25 SiO_2-700 H_2O. Synthesis temp.: 443 K.

The crystallization kinetics for the Al- and Fe-substituted mordenite samples are shown in Fig. 2. The percent crystallinity of the sample was determined by comparing the peak intensities at 2θ=9.79, 13.55, 22.37, 25.76, 26.39 and 27.81° to those of the most crystalline zeolite sample obtained. All the curves exhibit a typical sig-

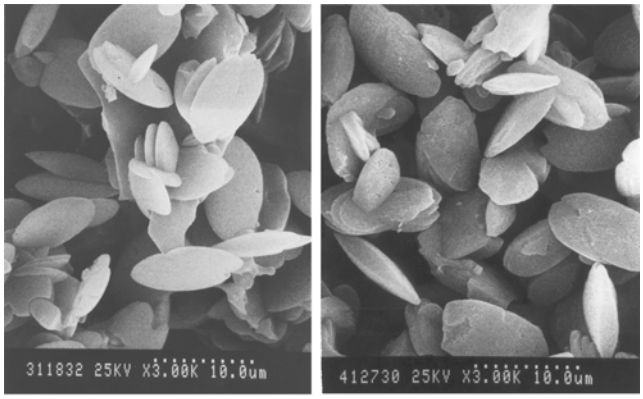

Fig. 3. SEM photographs of the (a) Al- and (b) Fe-substituted mordenite crystals.

moidal nature, characteristic of both the sequential processes of nucleation and crystal growth. The overall crystallization rates at constant gel composition and temperature decreased with increasing iron content of the synthesis gel. The increase in iron content in the synthesis gel was found to cause a decrease in the rate of nucleation (longer induction period) and to extend the crystallization period needed to obtain fully crystalline sample.

Fig. 3 shows the SEM photograph of the as-synthesized Al- and Fe-substituted mordenite crystals. These samples appear under the scanning microscope as uniform oval or discus-shaped crystals of size about 10 and 11 μm, respectively. No distinct change in morphology was observed on increasing the iron content.

IR spectra of normal Al- and partially Fe-substituted mordenite are shown in Fig. 4. The IR spectrum for mordenite closely matches that reported in the literature [31]. Partially Fe-substituted mordenite showed a pattern similar to the one corresponding to normal Al-mordenite. In these spectra, the absorption bands originating from iron hydroxides and iron oxides were not observed. Upon introducing Fe in the zeolite framework, IR absorption bands shifted towards the lower frequency region compared with those of the iron free mordenite. The bands at 1,227 and 810 cm^{-1}, due to asymmetric and symmetric stretching vibrations of Si-O-T (T=Al), were shifted to 1,200 and 788 cm^{-1} on isomorphous substitution of Al by Fe atoms in the lattice framework. The shift to lower frequency in the spectra is due to increases in the unit cell parameters caused by Fe^{3+} existing on tetrahedral sites, and similar results for other ferrisilicates were reported earlier [32,33].

In zeolites, the closeness in mass between Si and Al does not give rise to distinct contributions from the -(Si-O-Si)$_n$- and -(Si-O-Al)$_n$- vibrations [34]. However, in the ferrisilicate, silicon and iron are sufficiently different in atomic weight to change the reduced mass of the harmonic oscillator when iron is substituted for silicon. This difference can be sufficient to produce separate bands [35]. Accordingly, in the partially Fe-substituted mordenite, a new Si-O-Fe bond vibration could be found near 668 cm^{-1}, which is absent in the IR spectrum of normal mordenite. Szostak and Thomas [3,36] have found that the Si-O-Fe symmetric stretching vibration occurs at 679 and 656 cm^{-1} in the sodalite and ZSM-5 system, respectively. We also reported similar results previously that the absorption originating from the vibration of Fe-O-Si is observed at 668 cm^{-1} in the spectra of ferrisilicate LTL [37].

The use of ESR spectroscopy as a technique for detecting the presence of framework Fe^{3+} has been discussed by several authors [13,14,38,39], although the detailed interpretation of the ESR spectra is still a matter of debate [40]. Fig. 5 shows ESR spectra of the as-synthesized partially Fe-substituted mordenite. The ESR spectra of the sample reveal two signals: a sharp signal at g=4.3 assignable to tetrahedral Fe(III) [41] and a broad signal at g=2.0 assignable to octahedrally coordinated Fe^{3+} in non-framework positions. The enhanced intensity of the g=4.3 signal at lower temperature as well as its relative insensitivity to oxidation-reduction treatments suggests that it arises from Fe^{3+} ions in tetrahedral lattice positions rather than non-framework positions. Just about every work [38-42] dealing with Fe-substitution in molecular sieves shows both g=4.3 and g=2.0 signals in the ESR spectra even when completely isomor-

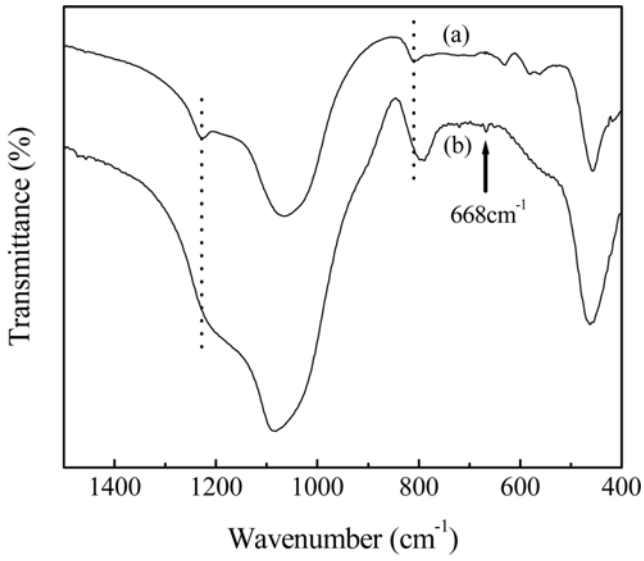

Fig. 4. IR spectra of (a) Al- and (b) Fe-substituted mordenite.

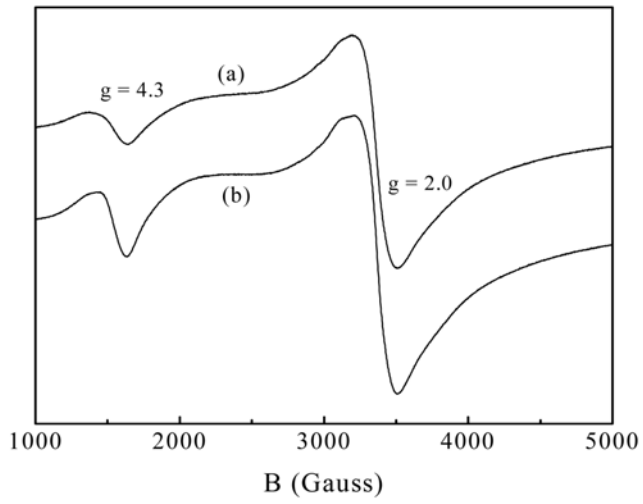

Fig. 5. ESR spectra of Fe-substituted mordenite at (a) 297 K and (b) 100 K.

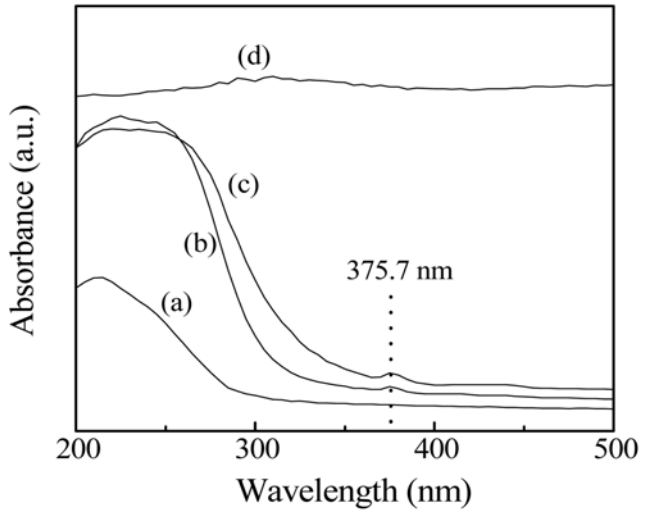

Fig. 6. UV-vis diffuse reflectance spectra of the as-synthesized Fe-substituted mordenite samples. (a) x=0.00, (b) x=0.15, (c) x=0.30, and (d) Fe_2O_3 powder.

phous substitution is claimed, and their relative size and variation with the iron concentration also vary depending on the zeolite system. ESR is predominantly used to check the g=4.3 signal in order to confirm the tetrahedral substitution. The signal at g=2.0 is known to be strongly affected by the water vapor content, and Park and Chon [41] reported that it diminishes with water vapor for FAPO-5, whereas it grows with water vapor for Fe-ZSM-5 [36].

The UV-vis spectra of the as-synthesized Fe-substituted mordenite samples with different iron content are shown in Fig. 6. A strong absorption band in the range of 200-300 nm is due to the charge transfer from ligand to isolated framework Fe^{3+} ions, while weak bands in the range of 370-450 nm are attributed to d−d transitions of Fe^{3+} ions [43,44]. In the spectra, absorption which was not observed in the UV spectra of normal Al-mordenite was observed at 375.7 nm, and the strength of this absorption band increases with increasing iron content of the sample. This absorption band is significantly different from the band pattern of Fe_2O_3 powder. Inui et al. [45] have reported that the absorptions in UV spectra appeared at 370, 405, and 435 nm for pentasil-type Fe-silicates. The results of UV obtained further confirm the isomorphous substitution of Fe^{3+} in the mordenite framework.

X-ray absorption spectroscopy (XAS) at the Fe K-edge was performed to collect information on the chemical state and the environment of Fe^{3+} in the partially Fe-substituted mordenite framework. XANES spectra of Fe-substituted mordenite samples above the Fe K-edge are shown in Fig. 7 after the normalization. Below the absorption edge, a pre-edge peak was found near 7,112 eV. It corresponds to transitions from 1 s to 3d-like levels [44]. In an octahedral environment, this peak is weak due to the presence of an inversion center [20] and two components are generally observed. In a tetrahedral environment, the pre-edge peak intensity is higher and only one single peak was found for Fe-containing glasses [46]. The qualitative information deduced from the XANES has been complemented by the EXAFS study. Fig. 8 shows the Fourier transformation (FT), which was performed from the region of $30<k<120$ nm^{-1} using the Hanning window function. The curve fitting result

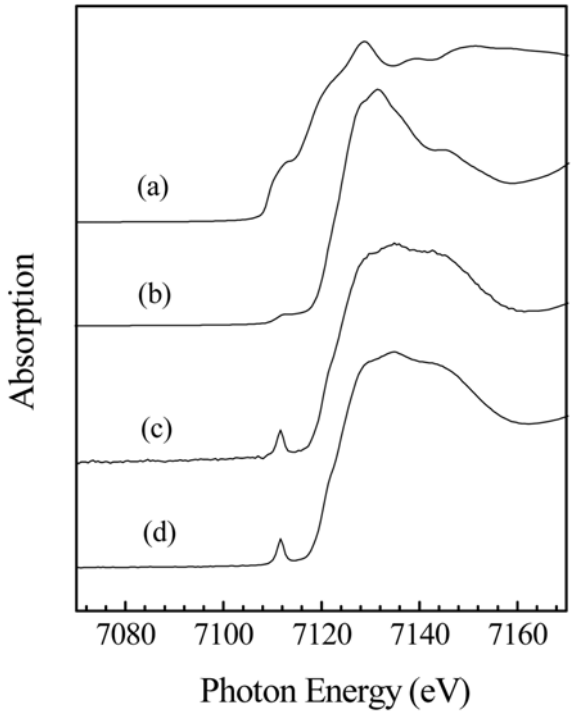

Fig. 7. XANES spectra of (a) Fe foil, (b) Fe_2O_3, (c) Fe-substituted mordenite (x=0.15), and (d) Fe-substituted mordenite (x=0.30).

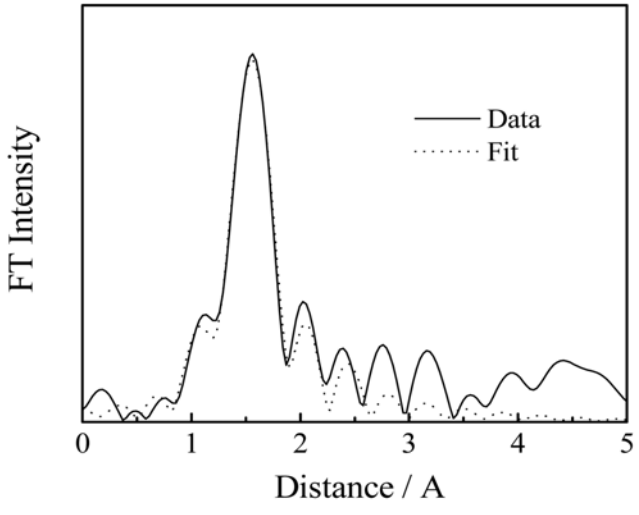

Fig. 8. Fourier transform of Fe-substituted mordenite. The best fitted theoretical EXAFS function is shown as the dotted line.

is shown as a dotted curve in Fig. 8. According to the XAS, the Fe-O distance and Fe-O coordination number for Fe-substituted mordenite (x=0.15) were 1.86 Å and 4.1, respectively. We have taken the data using a transmission mode in relatively short time, and its signal to noise ratio was sufficient enough to conduct the 1st shell calculations to estimate the Fe-O coordination number and its interatomic distance. Certainly, the Fe-O-Si(Al) coordination number and its distance would provide a more definite supporting evidence of the isomorphous Fe-substitution, but this type of calculation demands

Table 1. Activity for the alkylation of toluene with ethanol

Catalyst	H-Mordenite (x=0.00)	H-Fe-substituted Mordenite (x=0.30)
Conversion (mol%)	9.6	5.0
Product distribution (mol%)		
Benzene+C_6	2.2	4.7
Ethylbenzene	1.5	2.0
Xylene	10.3	10.0
Ethyltoluene	64.7	74.2
Trimethyltoluene	15.8	4.1
Diethyltoluene	5.5	5.0
Ethyltoluene isomer selectivity (mol%)		
Ortho	31.7	55.9
Meta	48.5	40.2
Para	19.8	3.9

Reaction condition: temp.: 623 K, WHSV=10, toluene/ethanol=2, TOS 2 h.

more efforts involving molecular modeling and it is necessary to take the data in a fluorescence mode, which requires substantially longer synchrotron radiation beam time. The XAS results overall indicate that the majority of the iron was substituted into the mordenite framework.

Finally, the toluene alkylation reaction with ethanol at 623 K under atmospheric pressure was conducted as a probe reaction. The catalytic activity and selectivity data of the Al- and Fe-substituted mordenite samples for toluene alkylation are presented in Table 1. The activity in terms of toluene conversion with Fe-substituted mordenite was lower compared with that of the normal Al-mordenite, as expected from the decreased acid strength of the former [47]. In this case, the large reduction in conversion may also be a consequence of Fe^{3+} released from the zeolite structure blocking the unidimensional pores at high calcination/pretreatment temperature (773 K). Further investigations are in progress. For the Fe-substituted mordenite, the ethyltoluene selectivity in product distribution seems enhanced, whereas the xylene selectivity is almost similar for both the samples. In this probe reaction study, however, a comparison of selectivity was not conducted at the same conversion level. It can be speculated that the modification of mordenite through isomorphous Fe^{3+} substitution resulted in substantial reduction of acid strength, and consequently the alkylation was promoted at the weakened acid sites. Disproportionation of toluene, which requires strong acid sites, cannot proceed due to weak acidity.

CONCLUSIONS

Isomorphous substitution of Fe^{3+} into mordenite was successfully carried out hydrothermally from the substrates in the composition range:

7 Na_2O-x Fe_2O_3-(1−x) Al_2O_3-25 SiO_2-700 H_2O,
where x=0, 0.15 and 0.3.

The overall crystallization rates at constant gel composition and temperature decreased with increasing iron content of the synthesis gel. The mid range IR spectra show a band shift to lower frequencies as the Fe^{3+} ions into the lattice incorporate, and a new Si-O-Fe bond vibration is located near 668 cm^{-1}. The ESR spectra show a signal at g=4.3, which can be assigned to Fe^{3+} isomorphously substituted in the tetrahedral positions. EXAFS at the Fe K-edge revealed that the Fe^{3+} ions were present in the zeolite framework in a four-fold coordination with an average Fe-O distance of 1.86 Å. In the UV-vis spectra, the absorption at 375.7 nm was observed only for the Fe-substituted mordenite samples. A toluene alkylation probe reaction study indicated that lattice iron species in mordenite weakened the acid strength and the ethyltoluene selectivity was enhanced as a result.

Therefore, it is believed that isomorphous substitution of Fe^{3+} for Al^{3+} in the crystalline lattice of mordenite has been satisfactorily demonstrated.

ACKNOWLEDGMENTS

This research was supported by a grant (code DD2-101) from the Carbon Dioxide Reduction & Sequestration Research Center, one of the 21st Century Frontier Programs funded by the Ministry of Science and Technology of Korean government.

REFERENCES

1. M. Dong, J. Wang, Y. Sun, T. Hu, T. Liu and Y. Xie, *Acta Chim. Sinica*, **43**, 237 (2001).
2. H.-Y. Chen, E.-M. El-Malki, X. Wang, R. A. Van Santen and W. M. H. Sachtler, *J. Mol. Catal. A: Chem.*, **162**, 159 (2000).
3. R. Szostak and T. L. Thomas, *J. Chem. Soc., Chem. Commun.*, 113 (1986).
4. P. Fejes, I. Kiricsi, K. Kovacs, K. Lazar, I. Marsi, A. Oszko, A. Rockenbauer and Z. Schay, *Appl. Catal. A: General*, **223**, 147 (2002).
5. F. Testa, L. Pasqua, F. Crea, R. Aiello, K. Lazar, P. Fejes, P. Lentz and J. B. Nagy, *Microporous and Mesoporous Materials*, **57**, 57 (2003).
6. J. A. Melero, G. Calleja, F. Martinez, R. Molina and K. Lazar, *Microporous and Mesoporous Materials*, **74**, 11 (2004).
7. G. J. Kim and W. S. Ahn, *Korean J. Chem. Eng.*, **9**, 60 (1992).
8. G. Giordano, A. Katovic and D. Caputo, *Stud. Surf. Sci. Catal.*, **140**, 307 (2001).
9. M. M. Mohamed, N. S. Gomaa, M. El-Moselhy and N. A. Eissa, *J. Colloid Interf. Sci.*, **259**, 331 (2003).
10. R. Kumar and P. Ratnasamy, *J. Catal.*, **121**, 89 (1990).
11. P. Ratnasamy and R. Kumar, *Catal. Today*, **9**, 327 (1991).
12. K. Lattam, C. I. Round and C. D. Williams, *Microporous and Mesoporous Materials*, **38**, 333 (2000).
13. V. Umamaheswari, W. Bohlmann, A. Poppl, A. Vinu and M. Hartmann, *Microporous and Mesoporous Materials*, **89**, 47 (2006).
14. J. Perez-Ramirez, J. C. Groen, A. Bruckner, M. S. Kumar, U. Bentrup, M. N. Debbagh and L. A. Villaescusa, *J. Catal.*, **232**, 318 (2005).
15. A. Ristic, N. N. Tusar, G. Vlaic, I. Arcon, F. Thibault-Starzyk, N. Malicki and V. Kaucic, *Microporous and Mesoporous Materials*, **76**, 61 (2004).
16. A. Ristic, N. N. Tusar, I. Arcon, N. Z. Logar, F. Thibault-Starzyk, J. Czyzniewska and V. Kaucic, *Chem. Mater.*, **15**, 3643 (2003).
17. N. S. Nesterenko, O. A. Ponomoreva, V. V. Yuschenko, I. I. Ivanova,

F. Testa, F. D. Renzo and F. Fajula, *Appl. Catal. A: General*, **254**, 261 (2003).
18. W. Zhao, L. Kong, Y. Luo and Q. Li, *Microporous and Mesoporous Materials*, **100**, 111 (2007).
19. M. S. Kumar, J. Perez-Ramirez, M. N. Debbagh, B. Smarsly, U. Bentrup and A. Bruckner, *Appl. Catal. B: Environmental*, **62**, 244 (2006).
20. Y. Han, X. Meng, H. Guan, Y. Yu, L. Zhao, X. Xu, X. Yang, S. Wu, N. Li and F. S. Xiao, *Microporous and Mesoporous Materials*, **57**, 191 (2003).
21. N. N. Tusar, N. Z. Logar, I. Arcon, G. Mali, M. Mazaj, A. Ristic, K. Lazar and V. Kaucic, *Microporous and Mesoporous Materials*, **87**, 52 (2005).
22. R. Aiello, J. B. Nagy, G. Giordano, A. Katovic and F. Testa, *C. R. Chimie*, **8**, 321 (2005).
23. T. Demuth, J. Hafner, L. Benco and H. Toulhoat, *J. Phys. Chem. B*, **104**, 4593 (2000).
24. S. Yuan, J. Wang, Y. Li and S. Peng, *J. Mol. Catal. A*, **175**, 131 (2001).
25. P. Fejes, J. B. Nagy, J. Halasz and A. Oszko, *Appl. Catal. A: General*, **175**, 89 (1998).
26. E. A. Stern, M. Newville, B. Ravel, B. Y. Yacoby and D. Haskel, *Physica B*, **208-209**, 117 (1995).
27. M. Newville, P. Livins, Y. Yacoby, J. J. Rehr, and E. A. Stern, *Phys. Rev. B*, **47**, 14126 (1993).
28. P. D. Angelo and M. Benfatto, *J. Phys. Chem. A*, **108**(20), 4505 (2004).
29. J. J. Rehr, R. C. Albers and S. I. Zabinsky, *Phys. Rev. Lett.*, **69**, 3397 (1992).
30. T. Lee, F. Benesch, Y. Jiang and C. G. Rose-Petruck, *Chem. Phys.*, **299**, 233 (2004).
31. G. J. Kim and W. S. Ahn, *Zeolites*, **11**, 745 (1991).
32. Y. Kuang, N. He, J. Wang, P. Xiao, C. Yuan and Z. Lu, *Colloids and Surfaces A: Physicochemical and Engineering Aspects*, **179**, 177 (2001).
33. V. Parvulescu and B.-L. Su, *Catal. Today*, **69**, 315 (2001).
34. E. M. Flanigen, in J. Rabo (Ed.), *Zeolite chemistry and catalysis*, Am.Chem. Soc., Washington DC, p. 201 (1971).
35. F. Hazel, R. U. Schock and M. Gordon, *J. Am. Chem. Soc.*, **71**, 2256 (1949).
36. R. Szostak and T. L. Thomas, *J. Catal.*, **100**, 555 (1986).
37. Y. S. Ko and W. S. Ahn, *Microporous and Mesoporous Materials*, **9**, 131 (1997).
38. P. Fejes, I. Kiricsi, K. Lazar, I. Marsi, A. Rockenbauer and L. Korecz, *Appl. Catal. A: General*, **242**, 63 (2003).
39. P. Decyk, M. Trejda and M. Ziolek, *C. R. Chimie*, **8**, 635 (2005).
40. D. Goldfarb, M. Barnardo, K. G. Strohmaier, D. E. W. Vaughan and H. Thomann, *J. Am. Chem. Soc.*, **116**, 6344 (1994).
41. A. Bruckner, U. Lohse and H. Mehner, *Microporous and Mesoporous Materials*, **20**, 207 (1998).
42. J. W. Park and H. Chon, *J. Catal.*, **133**, 159 (1992).
43. J. Perez-Ramirez, M. S. Kumar and A. Brukner, *J. Catal.*, **223**, 13 (2004).
44. G. Berlier, G. Spoto, S. Bordiga, G. Ricchiardi, P. Fisicaro, A. Zecchina, I. Rossetti, E. Selli, L. Forni, E. Giamello and C. Lamberti, *J. Catal.*, **208**, 64 (2002).
45. T. Inui, H. Nagata, T. Takeguchi, S. Iwamoto, H. Matsuda and M. Inoue, *J. Catal.*, **139**, 482 (1993).
46. F. Babonneau, S. Doeuff, A. Leaustic, C. Sanchez, C. Cartier and M. Verdaguer, *Inorg. Chem.*, **27**, 3166 (1988).
47. S. Yuan, J. Wang, Y. Li and H. Jiao, *J. Mol. Structure (Theochem)*, **674**, 267 (2004).